Title

Pervasive iron limitation at subsurface chlorophyll maxima of the California Current.

Journal

Proceedings of the National Academy of Sciences of the United States of America, 115(52)

ISSN

0027-8424

Authors

Hogle, Shane L
Dupont, Christopher L
Hopkinson, Brian M
et al.

Publication Date

2018-12-01

DOI

10.1073/pnas.1813192115

Peer reviewed

Pervasive iron limitation at subsurface chlorophyll maxima of the California Current

Shane L. Hogle[a,b,1], Christopher L. Dupont[c], Brian M. Hopkinson[d], Andrew L. King[e], Kristen N. Buck[f], Kelly L. Roe[g], Rhona K. Stuart[h], Andrew E. Allen[a,c], Elizabeth L. Mann[i], Zackary I. Johnson[j], and Katherine A. Barbeau[a,1]

[a]Scripps Institution of Oceanography, University of California, San Diego, La Jolla, CA 92093; [b]Department of Civil and Environmental Engineering, Massachusetts Institute of Technology, Cambridge, MA 02139; [c]Microbial and Environmental Genomics, J. Craig Venter Institute, La Jolla, CA 92037; [d]Department of Marine Sciences, University of Georgia, Athens, GA 30602; [e]Section for Marine Biogeochemistry and Oceanography, Norwegian Institute for Water Research, NO-5006 Bergen, Norway; [f]College of Marine Science, University of South Florida, Tampa, FL 33620; [g]Department of Chemistry and Biochemistry, The College at Brockport, State University of New York, Brockport, NY 14420; [h]Biosciences and Biotechnology Division, Lawrence Livermore National Laboratory, Livermore, CA 94550; [i]Trace Metal Biogeochemistry Laboratory, Bigelow Laboratory for Ocean Sciences, East Boothbay, ME 04544; and [j]Marine Laboratory and Biology Department, Duke University, Beaufort, NC, 28516

Edited by David M. Karl, University of Hawaii, Honolulu, HI, and approved November 7, 2018 (received for review August 1, 2018)

Subsurface chlorophyll maximum layers (SCMLs) are nearly ubiquitous in stratified water columns and exist at horizontal scales ranging from the submesoscale to the extent of oligotrophic gyres. These layers of heightened chlorophyll and/or phytoplankton concentrations are generally thought to be a consequence of a balance between light energy from above and a limiting nutrient flux from below, typically nitrate (NO_3). Here we present multiple lines of evidence demonstrating that iron (Fe) limits or with light colimits phytoplankton communities in SCMLs along a primary productivity gradient from coastal to oligotrophic offshore waters in the southern California Current ecosystem. SCML phytoplankton responded markedly to added Fe or Fe/light in experimental incubations and transcripts of diatom and picoeukaryote Fe stress genes were strikingly abundant in SCML metatranscriptomes. Using a biogeochemical proxy with data from a 40-y time series, we find that diatoms growing in California Current SCMLs are persistently Fe deficient during the spring and summer growing season. We also find that the spatial extent of Fe deficiency within California Current SCMLs has significantly increased over the last 25 y in line with a regional climate index. Finally, we show that diatom Fe deficiency may be common in the subsurface of major upwelling zones worldwide. Our results have important implications for our understanding of the biogeochemical consequences of marine SCML formation and maintenance.

nutrient limitation | iron | light | California Current | deep chlorophyll maximum

Fe and light are essential for phytoplankton photosynthesis, but both resources are scarce in much of the ocean. Surface ocean primary productivity is limited by the availability of Fe in some regions (1), and mesoscale Fe fertilization experiments now firmly demonstrate that Fe availability controls phytoplankton biomass and growth rates in the Southern, equatorial Pacific, and subarctic Pacific oceans (2). In addition, phytoplankton Fe limitation has been observed in midlatitude coastal upwelling zones (3, 4), throughout mesoscale circulation features (5, 6), and at the edge of subtropical gyres (7). In the surface ocean light attenuates rapidly to less than 1% of incident photosynthetically available radiation ($z_{1\%}$) at depths from 50 m to 200 m, depending on turbidity. However, many diverse phytoplankton groups have adapted to growth at depths approaching $z_{1\%}$ despite the challenging low-light conditions. Prior studies noting the overlapping scarcity of Fe and light in much of the ocean predicted that these two resources synergistically colimit phytoplankton growth (8), particularly in subsurface chlorophyll maximum layers (SCMLs) (9). Indeed, work with cultured phytoplankton demonstrates that Fe/light colimitation can arise when demand for Fe-rich photosynthetic redox proteins increases under low-light conditions (9, 10). However, the potential for phytoplankton Fe or Fe/light (co)limitation in SCMLs has been explored only in a handful of field studies despite the significant feedbacks linking Fe/light (co)limitation, dust deposition, and oceanic CO_2 uptake in global biogeochemical models (11). Although Fe/light colimitation has been observed in some high-latitude SCMLs (12, 13), mid-/low-latitude SCMLs from both coastal and pelagic zones remain understudied. Dissolved Fe minima at SCMLs from the subtropical North Pacific gyre (14) and the Sargasso Sea (15) may be a consequence of intense biological demand, even Fe limitation, during summer months. One study documented phytoplankton Fe/light colimitation from mesotrophic and oligotrophic SCMLs in the California Bight and the eastern tropical North Pacific (16), while another found SCMLs in the oligotrophic Western Pacific to be mostly light limited with some groups of microbial eukaryotes potentially

Significance

The vertical distribution of phytoplankton cells and chlorophyll concentrations throughout the sunlit water column is rarely uniform. In many ocean regions, chlorophyll concentrations peak in distinct and persistent layers deep below the surface called subsurface chlorophyll maximum layers (SCMLs). SCML formation is hypothesized to reflect the consequences of phytoplankton light/macronutrient colimitation, behavior, and/or photoacclimation. We discovered unexpectedly persistent and widespread phytoplankton iron limitation and iron/light colimitation in SCMLs of the California Current and at the edge of the North Pacific Subtropical Gyre using shipboard incubations, metatranscriptomics, and biogeochemical proxies. These results suggest that interactions and feedbacks between iron and light availability play an important and previously unrecognized role in controlling the productivity and biogeochemical dynamics of SCMLs.

Author contributions: S.L.H., C.L.D., B.M.H., K.N.B., E.L.M., Z.I.J., and K.A.B. designed research; S.L.H., C.L.D., B.M.H., A.L.K., K.N.B., K.L.R., R.K.S., E.L.M., Z.I.J., and K.A.B. performed research; S.L.H. contributed new reagents/analytic tools; S.L.H., C.L.D., B.M.H., A.L.K., K.N.B., E.L.M., Z.I.J., and K.A.B. analyzed data; and S.L.H., C.L.D., B.M.H., A.L.K., K.N.B., K.L.R., R.K.S., A.E.A., E.L.M., Z.I.J., and K.A.B. wrote the paper.

The authors declare no conflict of interest.

This article is a PNAS Direct Submission.

Data deposition: All data supporting the findings of this study are available at the following websites: CalCOFI time series data have been deposited in the CalCOFI data archives, new.data.calcofi.org/index.php/reporteddata. Metatranscriptome and metagenome biological sequence files have been deposited in iMicrobe, https://imicrobe.us (iMicrobe project ID: CAM_P_0001069). Biogeochemical data subsets, metatranscriptome annotations, and all computer code required to reproduce the results reported in this study have been deposited in Zenodo, https://doi.org/10.5281/zenodo.1495558 and https://doi.org/10.5281/zenodo.1495504. Unprocessed biogeochemical data have been deposited in the UCSD Datazoo Research Project, oceaninformatics.ucsd.edu/datazoo/catalogs/ccelter/sources/1758.

[1]To whom correspondence may be addressed. Email: shogle@mit.edu or kbarbeau@ucsd.edu.

This article contains supporting information online at www.pnas.org/lookup/suppl/doi:10.1073/pnas.1813192115/-/DCSupplemental.

Published online December 10, 2018.

exhibiting Fe/light colimitation (17). However, studies using multiple complementing experimental approaches at varied scales are needed to establish the prevalence of phytoplankton Fe limitation or Fe/light colimitation within SCMLs worldwide.

High primary productivity in the southern California Current (CC) and other Eastern Boundary Current systems is supported by intense upwelling of macronutrient-rich waters (18). However, local variation in Fe concentrations and other biogeochemical factors can generate Fe-limited phytoplankton communities in the CC (4, 19). During July 2007 we investigated the role of Fe and light as (co)limiting factors along a transect of California Cooperative Oceanic Fisheries Investigations (CalCOFI) line 93.3 (*SI Appendix*, Fig. S1), which spans the inshore (~0–150 km offshore), transition (~150–450 km offshore), and offshore (~450 km offshore) zones of the southern CC (20). In addition to sampling all standard CalCOFI stations on this transect, we intensively sampled three stations (93.3/40, 93.3/80, and 93.3/120) representing the inshore, transition, and offshore zones, respectively. At these three stations we measured total dissolved Fe (dFe) concentrations and the concentrations of strong, organic Fe-binding ligands (L_1). L_1 concentrations are positively correlated with Fe-limited phytoplankton growth in incubation studies, suggesting that phytoplankton and/or associated bacteria may actively produce L_1 as an adaptation to Fe limitation (21, 22). We also determined two other biogeochemical proxies for Fe deficiency: the NO_3 to dFe ratio (N:dFe) and Si_{ex}. Fe is likely to be a proximate limiting or colimiting nutrient in waters where the N:dFe ratio is greater than ~8 μmol/nmol (4, 19). At or above this threshold residual NO_3 accumulation in the water column can be attributed to the direct or indirect suppression of phytoplankton NO_3 utilization by low Fe availability (*SI Appendix*, section 4). Si_{ex} ($\mu mol \cdot L^{-1}$) is a modified form of the Si^* proxy (23) and traces shifts in the elemental composition of diatoms as a result of Fe deficiency (24) (*SI Appendix*, section 13). Negative Si_{ex} values in the water column indicate preferential diatom uptake of H_4SiO_4 relative to NO_3 due to Fe deficiency. Si_{ex} and the N:dFe ratio were negatively correlated across all samples ($\rho = -0.75$, $P = 2.4e\text{-}7$), indicating that low Si and high NO_3 waters generally also had low dFe concentrations, consistent with Fe-limiting conditions for diatoms (*SI Appendix*, Fig. S2). Si_{ex} increased substantially upon addition of Fe and Fe + light to inshore and transition zone SCML incubations (*SI Appendix*, Fig. S3), further emphasizing the proxy's responsiveness to the Fe status of the aggregate phytoplankton community.

At each of the intensively sampled stations we conducted incubation experiments with factorial resource additions of Fe, light, and combined Fe + light to SCML water. We measured chlorophyll *a* concentrations, primary production rates, the photochemical quantum efficiency of photosystem II (Fv/Fm), NO_3 consumption over the course of the incubations, and phytoplankton community composition by microscopy. Using these measurements we then classified incubation responses as simultaneous colimitation, independent colimitation, or serial limitation (25) (*SI Appendix*, section 11). Community transcriptomes were collected and sequenced from SCML and surface waters and were introduced in a prior publication (26). Here we focus on expression patterns of phytotransferrin (pTF), formerly known as ISIP2A (27, 28), and of iron stress-inducible protein 3 (ISIP3), which are diagnostic biosignatures of algal Fe stress in culture (29, 30) and in the field (31, 32).

Results and Discussion

Fe Limitation at SCMLs of the Inshore CC Sector. Biogeochemical proxies (Si_{ex} and N:dFe ratio), community transcriptomes, and incubation experiments consistently pointed to significant diatom Fe limitation at inshore SCMLs and were indicative of serial or single Fe limitation rather than colimitation (25). Fe concentrations were low in the surface mixed layer (mean of 0.10 $nmol \cdot L^{-1}$) and the depths of the ferricline (74 m) and nitracline (31 m) were strongly decoupled at station 93.3/40 (Fig. 1*A* and *SI Appendix*, Table S1). L_1 concentrations peaked at the SCML, N:dFe ratios were strikingly elevated ($N{:}dFe_{max}$ = 120 μmol/nmol) within the SCML, and the Si_{ex} profile mirrored that of N:dFe (Fig. 1*B*). The SCML incubation experiments displayed a five- to sevenfold increase in total chlorophyll *a* (Chl *a*), an ~2.5-fold increase in bulk NO_3 consumption, and an approximately twofold increase in Fv/Fm over the control in response to added Fe and Fe + light. The control and added light conditions were statistically indistinguishable (Fig. 2 and *SI Appendix*, Fig. S3). Primary production rates increased the most (2.5- to fivefold over control) with added Fe + light and Fe, while light alone had no effect. Large chain-forming diatoms dominated in added Fe and Fe + light incubation conditions (*SI Appendix*, Fig. S4). ISIP3 and pTF transcripts were strikingly abundant relative to other protein functional families in community transcriptomes from the SCML at station 93.3/40 with transcripts from four taxonomic groups exceeding the 95th rank percentile of all taxonomically aggregated community transcripts (Fig. 3). *Phaeocystis* and pelagophytes were two of the most abundant taxonomic groups detected at 93.3/40 (*SI Appendix*, Fig. S5), and pTFs belonging to these groups were in the top 1% of all identifiable *Phaeocystis* and pelagophyte transcripts/isoforms as well as the top 1% of all taxonomically aggregated community transcripts. Indeed, the expression of pTF/ISIP3 by diatoms, dinoflagellates, pelagophytes, and *Phaeocystis* often rivaled or exceeded that of highly expressed genes for essential cellular functions from each taxonomic group including ribosomal assembly proteins, NO_3 transporters, heat-shock–like proteins, and photosynthesis-related proteins (Fig. 3). Proteorhodopsin-like genes, which have recently been proposed as an alternative, Fe-independent energy acquisition strategy for iron-limited diatoms (33), were some of the most highly expressed diatom transcripts at the SCML of 93.3/40—perhaps also due to Fe stress. These expression patterns suggest that inshore SCML phytoplankton were investing significant resources into cellular pathways for managing Fe deficiency.

Fe/Light Colimitation at the CC Transition and Offshore Zones. At the oligotrophic edge of the transition zone and in the offshore zone we observed a deepening of the nitracline and SCML toward the base of the euphotic zone where low light levels may have increased photosynthetic Fe demand to the point of Fe/light colimitation. SCMLs at stations 93.3/80 and 93.3/120 displayed multiple signatures of potential Fe/light colimitation. dFe concentrations were again low in the surface mixed layer (mean of 0.13 $nmol \cdot L^{-1}$ and 0.11 $nmol \cdot L^{-1}$ in the transition and offshore zones, respectively) and the depths of the ferricline and nitracline were strongly decoupled at station 93.3/120 and moderately offset at station 93.3/80 (Fig. 1*A*). We observed a localized Fe depletion at the outer transition zone SCML, potentially due to enhanced localized biological Fe uptake. We also measured a localized L_1 increase at the offshore zone SCML, consistent with enhanced biological production of Fe acquisition molecules at this depth. N:dFe ratios greater than 8 μmol/nmol and negative Si_{ex} values highlighted the base of the SCML as a region of potential diatom Fe deficiency in most of the transition zone (Fig. 1*B*). In the offshore zone, negative Si_{ex} tracked the $\sigma_\theta = 26\ kg \cdot m^{-3}$ isopycnal to depths 100 m below the euphotic zone (Fig. 1*C*), indicating that the signal may not have been from local diatom Fe deficiency and potentially Fe-limited waters advected from elsewhere (*SI Appendix*, section 13C.2). In this sector mesoscale circulation features (6, 34) and wind-stress curl upwelling (35) are likely important sources of new N to the euphotic zone but may be too infrequent to generate chronic Fe-limited diatom growth and a persistent Si_{ex} signal at the SCML.

The outer transition zone incubation responses at 93.3/80 were most consistent with independent Fe/light colimitation (*SI Appendix*, section 11). Fe + light stimulated the greatest NO_3 drawdown (fourfold over control), primary production (15-fold

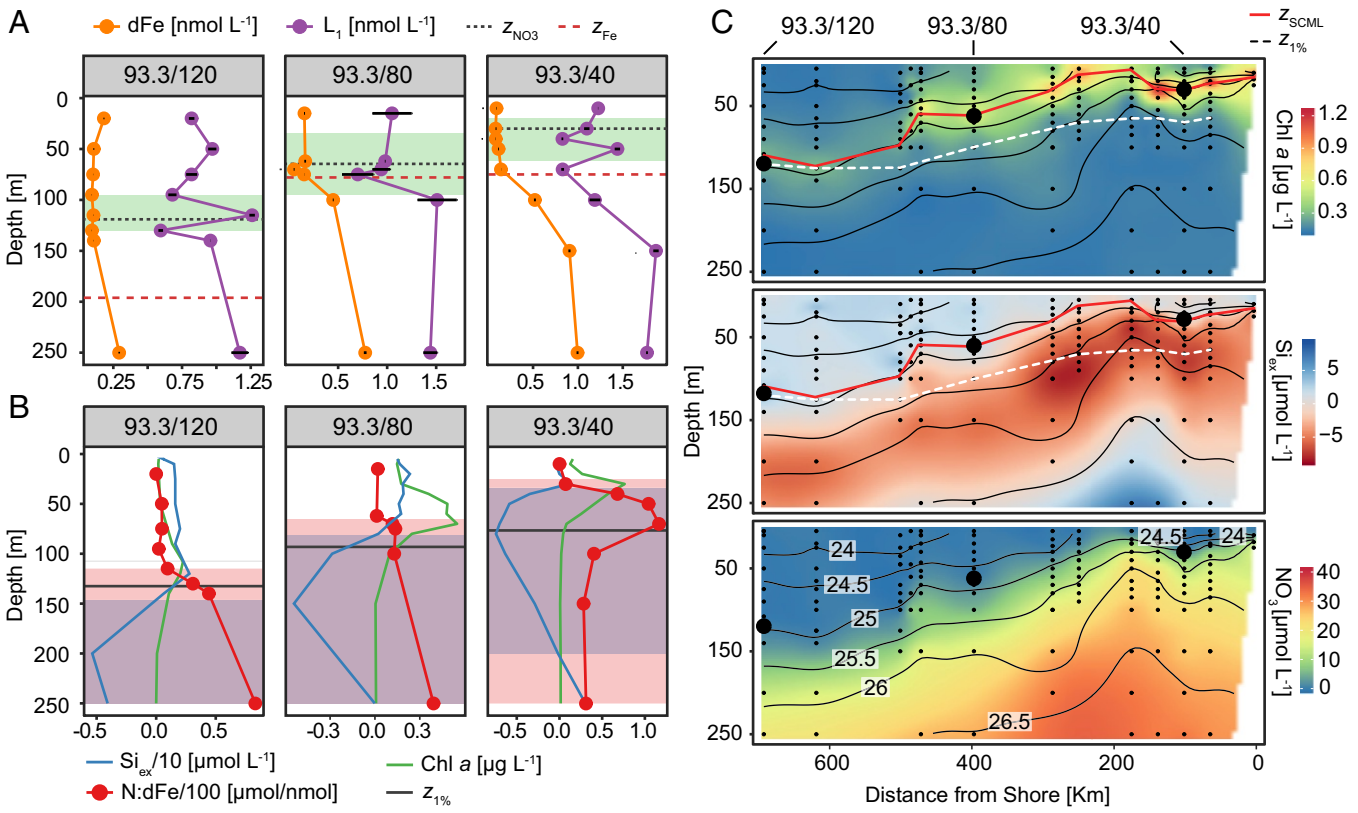

Fig. 1. (*A*) Profiles of dissolved Fe (orange) and L_1 (purple) concentrations. The green box denotes depths where chlorophyll *a* (Chl *a*) is within 50% of the concentration at the SCML depth (z_{SCML}), the dashed black line is nitracline depth (z_{NO_3}), and the dashed red line is ferricline depth (zFe) (*SI Appendix*, Table S1 and section 4). (*B*) Profiles of Chl *a* (green), Si_{ex}/10 (blue), and N:dFe/100 (red). The black line represents the depth of 1% of incident irradiance ($z_{1\%}$). Red (N:dFe $\geq$ 8), blue ($Si_{ex} < 0$), and purple (both proxies) indicate depth ranges with potential diatom Fe deficiency. (*C*) Chl *a*, NO_3, and Si_{ex} (26.5 kg·m^{-3} source isopycnal) sections. Potential density anomaly (σ_θ) contours are in black. Small circles show nutrient sampling depths and large circles show incubation and metatranscriptome depths. White and red dashed lines show $z_{1\%}$ and z_{SCML}, respectively.

over control), and total Chl *a* (5.5-fold over control) increases, while responses to Fe or light alone were similar to each other and significantly smaller than for Fe + light. However, the single addition of iron or light significantly enhanced NO_3 drawdown (Fe, 1.7-fold over control; light, 1.5-fold over control) and the addition of iron significantly increased the Chl *a* concentration (2.5-fold over control). Large chain-forming diatoms dominated incubation responses to added Fe + light (*SI Appendix*, Fig. S4), while iron-stress transcripts were in the top 1% of all expressed *Phaeocystis* and pelagophyte genes in situ (Fig. 3). Incubation experiments from 93.3/120 displayed a roughly twofold increase in diatom cell numbers, NO_3 drawdown, Chl *a* concentrations, and primary production in Fe + light conditions over the control (Fig. 2). Only the increase in Chl *a* was statistically significant, but it was challenging to detect significant differences in the means across incubation replicates because responses in the offshore zone were substantially smaller and noisier than in other regions. Given this caveat, our results suggest a potential for simultaneous Fe/light colimitation in oligotrophic SCMLs in the offshore zone. Smaller non–chain-forming diatoms were the dominant responders to the offshore zone Fe addition incubations (*SI Appendix*, Fig. S4), and the in situ positive Si_{ex} signal at the offshore SCML suggests that heavily silicified, Fe-limited forming diatoms were not abundant at the time of sampling. Indeed, pelagophytes numerically dominated the metatranscriptomes at 93.3/120, and pelagophyte ptF/ISIP3 transcripts were in the top 1% of all expressed transcripts in the metatranscriptome and in the top 0.1% of pelagophyte transcripts indicating significant cellular resource investment into Fe acquisition by small, nonsilicifying phytoplankton.

SCML Fe Deficiency Estimated from a 40-y Time Series. We sought to characterize the potential for diatom Fe deficiency in the southern CC across broader spatial and temporal scales by leveraging 40 y of monthly sampling data collected from 75 stations distributed over a 190,000-km^2 area as a part of the CalCOFI program (calcofi.org/). We used Si_{ex} as a biogeochemical proxy for diatom Fe deficiency because H_4SiO_4 and NO_3 measurements are readily available in the CalCOFI dataset and there is a strong correlation between negative Si_{ex} and experimentally determined Fe limitation in our results (Figs. 1 and 2 and *SI Appendix*, Fig. S3) and the results of others (5, 6, 24). The Si_{ex} tracer assumes minimal effects from horizontal mixing/advection, shifts in upwelling source depth, and other processes (nitrification, denitrification, variability in Si:N remineralization ratios) that may integrate nonspecific biogeochemical signals. In most settings, such as in the euphotic zone of the CC, these assumptions appear to be valid, but we note that in other biogeochemical regimes they may not be. In all test cases and datasets we examined Si_{ex} performed as a robust tracer (*SI Appendix*, section 13A).

During the spring and summer months over the last 40 y at least 30% of all SCML samples in the southern CC were Fe deficient to some degree ($Si_{ex} < 0$). Fe deficiency is disproportionately concentrated in SCMLs from the inshore (43% negative) and transition zones (26% negative) compared with the offshore zone (7% negative) (Fig. 4 and *SI Appendix*, Fig. S6). On average Si_{ex} from inshore and transition zone SCMLs has steadily become more negative since 2000 in contrast to the general increase in the 1990s and most of the 1980s (*SI Appendix*, Fig. S7). We also find that the total spatial area of Fe-deficient SCMLs has significantly increased for the inshore

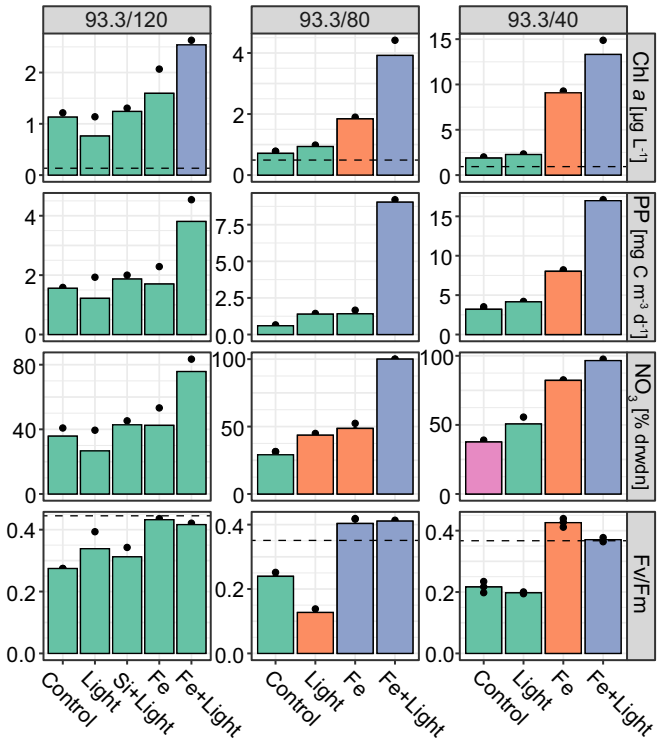

Fig. 2. Chl a, Primary production (PP), NO_3 drawdown (percentage of initial concentration), and Fv/Fm from the final time point of incubation experiments. Bars are means of replicate incubations (individual circles). Conditions in each experiment with group means that are statistically indistinguishable are colored the same. Different-colored conditions have statistically different means (ANOVA and pairwise *t* test with false discovery rate-corrected $P \leq 0.05$). At 93.3/120 we included a silicate + light incubation treatment to test for potential diatom silicate limitation (not detected). The lengths of incubations were 120 h, 168 h, and 216 h for 93.3/40, 93.3/80, and 93.3/120, respectively. The dashed horizontal line in the Chl *a* and Fv/Fm panels is the mean initial time-point measurement for the no addition control.

sector over the last 40 y (Fig. 4*E*). These trends have occurred in conjunction with a general shoaling of the SCML, the nitracline, and the euphotic zone in the southern CC (*SI Appendix*, Fig. S8) (20, 35, 36), particularly for the offshore and transition zones during the early 2000s. Negative Si_{ex} values often coincided with the highest observed Chl *a* concentrations in the inshore zone (*SI Appendix*, Fig. S6), suggesting a major contribution of Fe-deficient diatoms to coastal primary production. Negative Si_{ex} values in the offshore zone generally tracked the base of the euphotic zone (*SI Appendix*, Fig. S9) or extended below it (Fig. 1*A*). This signal may be caused by chronic in situ diatom Fe deficiency at the deepest parts of the offshore euphotic zone and/or may reflect along-isopycnal propagation of a negative Si_{ex} signal generated inshore as has been observed for other tracers (37, 38).

Patterns of Negative Si_{ex}, CC Winds, the North Pacific Gyre Oscillation, and Biogeochemical Variables. SCML Fe deficiencymay track decadal modes of climate variability in the southern CC. The North Pacific Gyre Oscillation (NPGO) mode is a regional climate index that is significantly correlated with fluctuations in the biogeochemistry and hydrography of the southern CC (39). Positive NPGO intervals (*SI Appendix*, Fig. S10) are associated with wind shifts that result in upwelling-favorable conditions in the CC (39) and coincide with the most extreme negative Si_{ex} events from the last 40 y (Fig. 4 and *SI Appendix*, Fig. S7). The strengthening of the NPGO amplitude since 1993 (39) also corresponds with a significant increase in the inshore spatial extent of diatom Fe deficiency at the SCML (Fig. 4*E*), potentially indicating shared forcing. However, the time-lagged correlations between Si_{ex} extent and wind-stress curl or Ekman-driven coastal upwelling rates are quantitatively weak ($\rho < 0.2$; *SI Appendix*, Fig. S11). This apparent weak correlation may actually reflect nonlinear (40) or cumulatively integrative (41) responses and does not necessarily exclude a mechanistic relationship between regional Si_{ex} trends at the SCML and decadal patterns of atmospheric forcing. Si_{ex} signals at southern CC SCMLs were moderately correlated with the difference between the nitracline and SCML depths ($\rho = 0.53, P <$ 1e-200) and the potential density at the SCML ($\rho = -0.49, P <$ 1e-200) (*SI Appendix*, Fig. S11). The positive correlation between Si_{ex} and the nitracline/SCML depth offset suggests that diatom Fe deficiency is associated with SCMLs that form below the top of the nitracline, which may reflect a mismatched stoichiometric supply of NO_3 and Fe from below. The negative correlation between Si_{ex} and SCML potential density may reflect an association with diatom Fe deficiency and increased isopycnal shoaling or upwelling strength in general.

Si_{ex} from a Global Perspective. To contextualize the pervasive Fe deficiency we observed at SCMLs from the southern CC, we

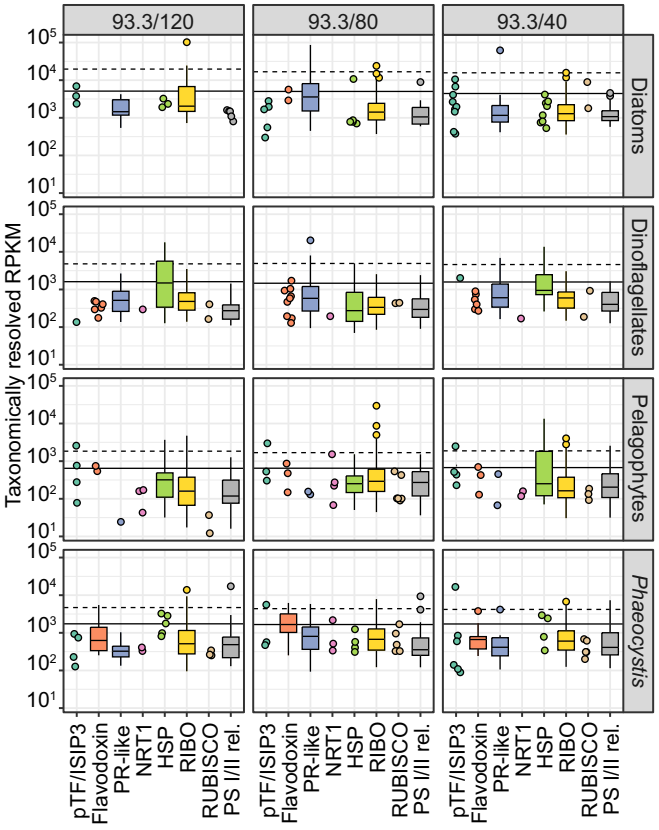

Fig. 3. Relative abundance of transcripts/isoforms from known iron-stress genes and genes related to essential cellular processes. The vertical axis (log10 scale) represents the reads per kilobase of transcript per million mapped reads to each of the four taxonomic groups at each station. Individual assembled transcripts/isoforms are binned into functional groups (horizontal axis). Functional groups with greater than 10 unique transcripts/isoforms are represented by boxplots; otherwise expression values for individual transcripts/isoforms are displayed. Individual transcripts/isoforms above the solid black lines exceed the taxonomic and library-specific 95th percentile ranking while those above the dashed line exceed the 99th percentile ranking and those in the lower 10% of percentile ranking are not included. HSP, heat-shock proteins; NRT1, nitrate transporter; PR-like, eukaryotic proteorhodopsin-like; PS I/II rel., photosystem reaction center proteins (PsbE, -F, -H–N, -R, -S, -W) and light-harvesting complex proteins (Chl *a*/*b*/*c* or fucoxanthin binding); RIBO, all ribosomal assembly protein subunits; RUBISCO, ribulose-1,5-bisphosphate carboxylase.

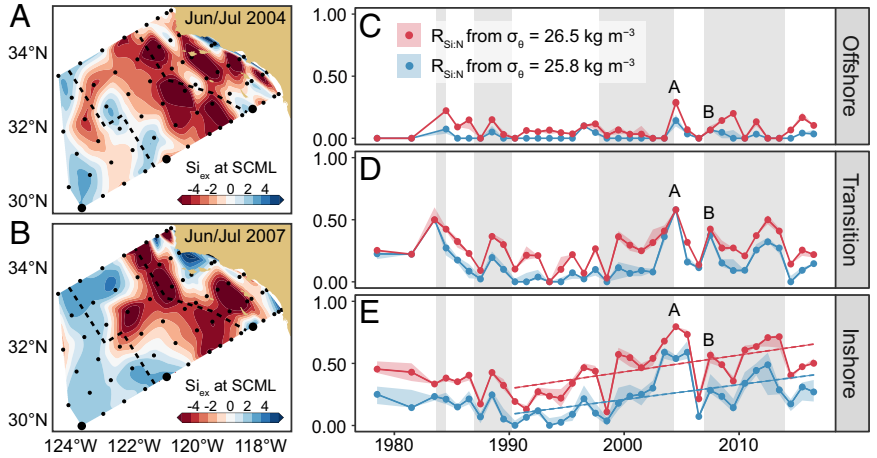

Fig. 4. Time series (1977–2017) of Si_{ex} (μmol·L^{-1}), at the SCML in the CalCOFI sampling area. (*A* and *B*) Interpolated values of Si_{ex} at the depth of the SCML for (*A*) June/July 2004 (season with most negative SCML Si_{ex} values) and (*B*) June/July 2007 (approximate time of cruise). Small circles depict CalCOFI sampling stations, while large circles display locations of incubations and metatranscriptomes. Dashed lines separate inshore–transition–offshore zones. (*C*–*E*) Average spring–summer (April–September) fraction of SCMLs with negative Si_{ex} for each zone. A and B time points in *C*–*E* correspond to the areal contour plots in *A* and *B*. Red and blue series show two different Si_{ex} estimates using a source upwelling isopycnal of 26.5 kg·m^{-3} and 25.8 kg·m^{-3}, respectively. (*E*) There is a significant monotonic increasing trend (nonparametric Mann–Kendall test $P < 0.002$) in the extent of negative Si_{ex} for the inshore region since 1990 (dashed lines are linear regressions for each source isopycnal). Shaded regions show when the NPGO index is positive.

also determined Si_{ex} at a global scale at 50 m depth using data from the 2013 World Ocean Atlas (42) (*SI Appendix*, section 6). Our results highlight the subsurface of coastal upwelling zones as potential hotspots of diatom Fe deficiency (Fig. 5). The CC (Figs. 4 and 5*A*) and the Humbolt/Peru Current (Fig. 5*B*) system show the largest negative Si_{ex} signals at 50-m depth, while the Benguela and Canary Currents (Fig. 5 *C* and *D*) display negative signals to a lesser extent. The Oman upwelling zone and the North Arabian Sea also appear to have notably Fe-deficient (Fig. 5*E*) Si_{ex} values in the subsurface. The greatest spatial extent of subsurface diatom Fe deficiency appears to overlap with well-known high-nutrient low-chlorophyll regions, such as the Subarctic North Pacific (43) and the Pacific equatorial upwelling zone (44). It is worth noting that many regions with negative Si_{ex} values identified in our analysis also overlie or potentially overlap with oxygen minimum zones (OMZs) and/or anoxic OMZs (45) where denitrification and anammox can decouple the cycling of H_4SiO_4 from NO_3 and may impart a nonspecific signal to Si_{ex}. However, the occurrence of denitrification/anammox above the upwelling source isopycnal would counter any signal of iron-limited diatom uptake and push Si_{ex} in a positive direction. Phytoplankton iron (co)limitation has been experimentally identified in surface waters from many of the negative Si_{ex} regions identified here (7, 43, 44, 46, 47), but few studies have investigated the potential for iron limitation at the depth ranges of SCMLs in these regions. We find that subsurface waters of many major oceanic upwelling regions display a biogeochemical imprint of diatom iron deficiency (negative Si_{ex}), which is consistent with our experimental and time series results from SCMLs in the CC.

Conclusions

The diagnosis of nutrient limitation in situ is a critical step toward better understanding fluxes of energy and matter in marine ecosystems. Our results suggest a strong coastal to offshore gradient in the combined effects of iron and light on SCML phytoplankton of the southern CC, a highly productive eastern boundary upwelling regime, and potentially upwelling zones worldwide (Fig. 5). The shallower inshore and inner transition zone SCML communities, which represent maxima in both diatom biomass and productivity, appear particularly susceptible to Fe limitation or Fe/light colimitation. It is less obvious whether deeper SCML communities from the oligotrophic offshore zones can be Fe deficient, but we do observe a significant effect of Fe + light on total Chl *a* concentrations and notably high expression of phytoplankton Fe-stress genes in situ. Based on our results we speculate that oligotrophic SCMLs may experience periods of Fe/light colimitation or Fe serial/single limitation, but further direct observations in the oligotrophic ocean are needed to confirm this hypothesis.

Persistent diatom Fe (co)limitation at SCMLs likely has downstream consequences for the carbon cycle. For example, increased diatom silicification may enhance particulate carbon export efficiency by increasing sinking rates and shielding cells from grazing in productive upwelling zones (5, 6). Furthermore, historical biogeochemical patterns of diatom iron deficiency at the CC subsurface appear to track dominant modes of climate variability in the North Pacific, which may be due to regional atmospheric patterns that decouple the nitracline, the ferricline, and the depth of the SCML. Biogeochemical models predict increased upwelling and NO_3 fluxes to the southern

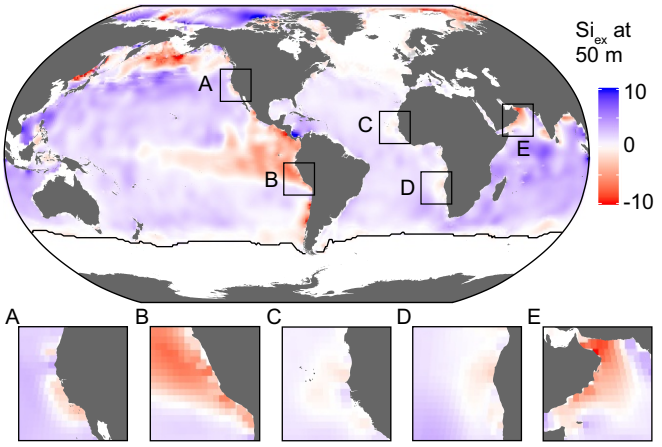

Fig. 5. Global distribution of Si_{ex} (μmol·L^{-1}) at 50-m depth relative to an upwelling source isopycnal of σ_θ = 26.5 kg·m^{-3}. Data are from the 1°-resolved annual (1955–2012) mean isosurface 2013 World Ocean Atlas. *A*–*E* highlight mean negative Si_{ex} upwelling regions. The solid black line in the Southern Ocean shows the outcropping of the σ_θ = 26.5 kg·m^{-3} isopycnal.

CC under anthropogenic climate change (48, 49), which may drive diatom communities at the SCML toward Fe limitation if the associated Fe fluxes do not increase proportionally. This potential atmospheric–biogeochemical linkage demonstrates a connection, mediated by iron, by which the changing climate may influence carbon cycling and primary productivity in SCMLs of the CC and potentially other eastern boundary currents.

Materials and Methods

Method details are available in *SI Appendix*. Samples for total dissolved iron concentrations, iron-binding ligand concentrations, and incubation experiments were collected and processed as described in refs. 4 and 24. Dissolved Fe was measured as in ref. 4 and Fe-binding ligands were measured as in ref. 50. The transcriptomic data (including all relevant methods) were introduced in a prior publication (26). Macronutrients were sampled using a rosette sampler and analyzed following the standard operating procedures from the California Current Ecosystem Long-Term Ecological Research program. Triplicate or duplicate 4-L incubations were conducted in acid-cleaned polycarbonate bottles, housed in a Percival incubator at 16 °C with a 12:12 light:dark cycle at a high- and low-light treatment and added Fe (*SI Appendix*, Table S3). Primary productivity and photophysiology were measured as described in refs. 17 and 26. CalCOFI and *World Ocean Atlas* hydrographic and nutrient data were downloaded from new.data.calcofi.org and https://www.nodc.noaa.gov. The Si_{ex} proxy (*SI Appendix*, section 13A) at SCML depths was calculated as $Si_{ex} = [\mu mol\ H_4SiO_4 \cdot L^{-1}] - ([\mu mol\ NO_3 \cdot L^{-1}] \times R_{Si:NO3})$, where $R_{Si:NO3}$ is the micromolar ratio of H_4SiO_4 to NO_3 at σ_θ = 25.8 kg·m^{-3}or 26.5 kg·m^{-3}.

ACKNOWLEDGMENTS. We thank the captain and crew of the *RV New Horizon*. We express our gratitude to members of the CalCOFI program and the Ocean Climate Laboratory at the National Oceanographic Data Center. We thank Melissa Carter for phytoplankton cell counts, the staff at the J. Craig Venter Institute (JCVI) for assistance with sequencing, and Dr. Thomas Hackl for assistance with computer code and two anonymous manuscript reviewers. Field work was funded by NSF Grant OCE-0550302 (to K.A.B. and E.L.M.) and NSF Grant 05-507098 (to Z.I.J.). K.A.B. acknowledges additional support from the California Current Ecosystem Long-Term Ecological Research Program (LTER NSF/OCE-0417616, OCE-1026607, and OCE-1637632). Metatranscriptomes are derived from the Global Ocean Sampling expedition and were funded through JCVI internal funds and the US Department of Energy (DOE), Office of Science, Office of Biological and Environmental Research (DE-FC02-02ER63453). A portion of this work was performed under the auspices of the US DOE by Lawrence Livermore National Laboratory under Contract DE-AC52-07NA27344.

1. Moore CM, et al. (2013) Processes and patterns of oceanic nutrient limitation. *Nat Geosci* 6:701–710.
2. Boyd PW, et al. (2007) Mesoscale iron enrichment experiments 1993-2005: Synthesis and future directions. *Science* 315:612–617.
3. Hutchins DA, Bruland KW (1998) Iron-limited diatom growth and Si:N uptake ratios in a coastal upwelling regime. *Nature* 393:561–564.
4. King AL, Barbeau K (2007) Evidence for phytoplankton iron limitation in the southern California current system. *Mar Ecol Prog Ser* 342:91–103.
5. Brzezinski MA, et al. (2015) Enhanced silica ballasting from iron stress sustains carbon export in a frontal zone within the California current. *J Geophys Res C Oceans* 120:4654–4669.
6. Stukel MR, et al. (2017) Mesoscale ocean fronts enhance carbon export due to gravitational sinking and subduction. *Proc Natl Acad Sci USA* 114:1252–1257.
7. Browning TJ, et al. (2017) Nutrient co-limitation at the boundary of an oceanic gyre. *Nature* 551:242–246.
8. Raven JA (1990) Predictions of Mn and Fe use efficiencies of phototrophic growth as a function of light availability for growth and of C assimilation pathway. *New Phytol* 116:1–18.
9. Sunda WG, Huntsman SA (1997) Interrelated influence of iron, light and cell size on marine phytoplankton growth. *Nature* 390:389–392.
10. Strzepek RF, Hunter KA, Frew RD, Harrison PJ, Boyd PW (2012) Iron-light interactions differ in Southern ocean phytoplankton. *Limnol Oceanogr* 57:1182–1200.
11. Nickelsen L, Oschlies A (2015) Enhanced sensitivity of oceanic CO2 uptake to dust deposition by iron-light colimitation. *Geophys Res Lett* 42:492–499.
12. Maldonado MT, Boyd PW, Harrison PJ, Price NM (1999) Co-limitation of phytoplankton growth by light and Fe during winter in the NE subarctic Pacific ocean. *Deep Sea Res Part 2 Top Stud Oceanogr* 46:2475–2485.
13. Boyd PW, et al. (2001) Control of phytoplankton growth by iron supply and irradiance in the subantarctic Southern ocean: Experimental results from the SAZ project. *J Geophys Res* 106:31573–31583.
14. Boyle EA, Bergquist BA, Kayser RA, Mahowald N (2005) Iron, manganese, and lead at Hawaii ocean time-series station ALOHA: Temporal variability and an intermediate water hydrothermal plume. *Geochim Cosmochim Acta* 69:933–952.
15. Sedwick PN, et al. (2005) Iron in the Sargasso sea (Bermuda Atlantic time-series study region) during summer: Eolian imprint, spatiotemporal variability, and ecological implications. *Glob Biogeochem Cycles* 19:GB4006.
16. Hopkinson BM, Barbeau KA (2008) Interactive influences of iron and light limitation on phytoplankton at subsurface chlorophyll maxima in the eastern north Pacific. *Limnol Oceanogr* 53:1303–1318.
17. Johnson ZI, et al. (2010) The effect of iron- and light-limitation on phytoplankton communities of deep chlorophyll maxima of the western Pacific ocean. *J Mar Res* 68:283–308.
18. Carr ME, Kearns EJ (2003) Production regimes in four eastern boundary current systems. *Deep Sea Res Part 2 Top Stud Oceanogr* 50:3199–3221.
19. Bruland KW, Rue EL, Smith GJ (2001) Iron and macronutrients in California coastal upwelling regimes: Implications for diatom blooms. *Limnol Oceanogr* 46:1661–1674.
20. Aksnes DL, Ohman MD (2009) Multi-decadal shoaling of the euphotic zone in the southern sector of the California current system. *Limnol Oceanogr* 54:1272–1281.
21. Rue EL, Bruland KW (1997) The role of organic complexation on ambient iron chemistry in the equatorial Pacific ocean and the response of a mesoscale iron addition experiment. *Limnol Oceanogr* 42:901–910.
22. Hogle SL, Bundy RM, Blanton JM, Allen EE, Barbeau KA (2016) Copiotrophic marine bacteria are associated with strong iron-binding ligand production during phytoplankton blooms. *Limnol Oceanogr Lett* 1:36–43.
23. Sarmiento JL, Gruber N, Brzezinski MA, Dunne JP (2004) High-latitude controls of thermocline nutrients and low latitude biological productivity. *Nature* 427:56–60.
24. King AL, Barbeau KA (2011) Dissolved iron and macronutrient distributions in the southern California current system. *J Geophys Res* 116:C03018.
25. Sperfeld E, Raubenheimer D, Wacker A (2015) Bridging factorial and gradient concepts of resource co-limitation: Towards a general framework applied to consumers. *Ecol Lett* 19:201–215.
26. Dupont CL, et al. (2015) Genomes and gene expression across light and productivity gradients in eastern subtropical Pacific microbial communities. *ISME J* 9:1076–1092.
27. McQuaid JB, et al. (2018) Carbonate-sensitive phytotransferrin controls high-affinity iron uptake in diatoms. *Nature* 555:534–537.
28. Morrissey J, et al. (2015) A novel protein, ubiquitous in marine phytoplankton, concentrates iron at the cell surface and facilitates uptake. *Curr Biol* 25:364–371.
29. Allen AE, et al. (2008) Whole-cell response of the pennate diatom *Phaeodactylum tricornutum* to iron starvation. *Proc Natl Acad Sci USA* 105:10438–10443.
30. Marchetti A, et al. (2017) Development of a molecular-based index for assessing iron status in bloom-forming pennate diatoms. *J Phycol* 53:820–832.
31. Chappell PD, et al. (2014) Genetic indicators of iron limitation in wild populations of *Thalassiosira oceanica* from the northeast Pacific ocean. *ISME J* 9:592–602.
32. Cohen NR, et al. (2017) Diatom transcriptional and physiological responses to changes in iron bioavailability across ocean provinces. *Front Mar Sci* 4:360.
33. Marchetti A, Catlett D, Hopkinson BM, Ellis K, Cassar N (2015) Marine diatom proteorhodopsins and their potential role in coping with low iron availability. *ISME J* 9:2745–2748.
34. Landry MR, et al. (2012) Pelagic community responses to a deep-water front in the California current ecosystem: Overview of the A-front study. *J Plankton Res* 34:739–748.
35. Rykaczewski RR, Checkley DM Jr (2008) Influence of ocean winds on the pelagic ecosystem in upwelling regions. *Proc Natl Acad Sci USA* 105:1965–1970.
36. Lindegren M, Checkley DM Jr, Ohman MD, Koslow JA, Goericke R (2016) Resilience and stability of a pelagic marine ecosystem. *Proc R Soc B Biol Sci* 283:20151931.
37. Bograd SJ, Mantyla AW (2005) On the subduction of upwelled waters in the California current. *J Mar Res* 63:863–885.
38. Gruber N, et al. (2011) Eddy-induced reduction of biological production in eastern boundary upwelling systems. *Nat Geosci* 4:787–792.
39. Di Lorenzo E, et al. (2008) North Pacific gyre oscillation links ocean climate and ecosystem change. *Geophys Res Lett* 35:L08607.
40. McGowan JA, et al. (2017) Predicting coastal algal blooms in southern California. *Ecology* 98:1419–1433.
41. Di Lorenzo E, Ohman MD (2013) A double-integration hypothesis to explain ocean ecosystem response to climate forcing. *Proc Natl Acad Sci USA* 110:2496–2499.
42. Garcia HE, et al. (2014) *World Ocean Atlas 2013, Vol 4: Dissolved inorganic nutrients (phosphate, nitrate, silicate)*. NOAA Atlas NESDIS 76, eds Levitus S, Mishonov A (NOAA, Silver Spring, MD), 25 p.
43. Boyd PW, et al. (2004) The decline and fate of an iron-induced subarctic phytoplankton bloom. *Nature* 428:549–553.
44. Martin JH, et al. (1994) Testing the iron hypothesis in ecosystems of the equatorial Pacific ocean. *Nature* 371:123–129.
45. Ulloa O, Canfield DE, DeLong EF, Letelier RM, Stewart FJ (2012) Microbial oceanography of anoxic oxygen minimum zones. *Proc Natl Acad Sci USA* 109:15996–16003.
46. Hutchins DA, et al. (2002) Phytoplankton iron limitation in the Humboldt current and Peru upwelling. *Limnol Oceanogr* 47:997–1011.
47. Moffett JW, et al. (2015) Biogeochemistry of iron in the Arabian sea. *Limnol Oceanogr* 60:1671–1688.
48. Bakun A, et al. (2015) Anticipated effects of climate change on coastal upwelling ecosystems. *Curr Clim Change Rep* 1:85–93.
49. Rykaczewski RR, Dunne JP (2010) Enhanced nutrient supply to the California current ecosystem with global warming and increased stratification in an earth system model. *Geophys Res Lett* 37:L21606.
50. Buck KN, Bruland KW (2007) The physicochemical speciation of dissolved iron in the Bering sea, Alaska. *Limnol Oceanogr* 52:1800–1808.